Coronal Solar Magnetism Observatory
Technical Note #16, Rev #3

Science Requirements of the COSMO K-Coronagraph

Joan Burkepile

Last Revised October 10, 2011

Summary

This technical note describes the scientific requirements of the K-coronagraph which is part of the COronal Solar Magnetism Observatory (COSMO). COSMO is a proposed facility dedicated to studying coronal and chromospheric magnetic fields and their role in driving solar activity such as coronal mass ejections (CMEs). COSMO is comprised of 3 instruments: a 1.5 m coronagraph to study coronal magnetic fields; a chromospheric and prominence magnetometer; and a K-coronagraph designed to study the formation of CMEs and the density structure of the low corona. To meet these goals, the COSMO K-coronagragh needs to acquire images of the white light corona in polarization brightness down to 1.05 solar radii ($R_\odot$) with a time cadence of 15 seconds to brightness levels of 10^{-9} $B_\odot$ at a signal-to-noise level of one. This technical note outlines the science drivers for the K-coronagraph. The major goals are: 1) to understand the formation of coronal mass ejections (CMEs) and their interaction with surrounding coronal structures and related activity (e.g. flares, prominence eruptions and shock waves); 2) identify Earth-directed CMEs (e.g. halos) in realtime, 3) determine the density distribution of the corona over solar cycle time scales; and 4) measure the radial brightness gradients beyond 1.5 $R_\odot$ in magnetically open regions. The COSMO K-coronagraph will replace the aging Mauna Loa Solar Observatory (MLSO) K-coronameter which has been in operation since 1980.

Introduction

The solar corona is a million-degree plasma which is the source of the solar wind and the site of explosive activity such as Coronal Mass Ejections (CMEs) that drive space weather throughout the heliosphere. The corona is organized by the Sun's magnetic field into brighter magnetically 'closed' regions, where the plasma is contained by the field, and magnetically 'open' regions of very low density where the plasma and field are carried outward to form the solar wind. Coronal brightness and the distribution of closed and open regions vary over the 11-year solar cycle as illustrated in Figure 1. This variation is driven by dynamo processes in the solar interior that determine the quantity and distribution of magnetic flux into the corona and drive the sunspot activity cycle.

Much of what is known about CME properties and the density structure of the corona comes from white light observations (e.g. Gosling et al. 1976, Howard et al. 1985, Hundhausen 1993, Hundhausen et al. 1994, St.Cyr et al. 1999, Yashiro et al. 2004,

Schmit et al. 2009). These observations are needed to understand CME formation, as well as the evolution of the global structure of magnetic field and density distribution of the corona. They also provide insight into the mechanisms responsible for coronal heating and solar wind acceleration. The Mauna Loa K-coronameter has been operating since 1980 and provides unique white light observations of the low corona. The K-coronameter utilizes a 1-D CCD detector to acquire scans of the low corona every ½ degree in azimuth and builds up an image of the corona over 360 degrees every 3 minutes. We discuss the scientific requirements for a new coronagraph to replace the Mauna Loa K-coronameter that will significantly improve our understanding of the formation and dynamics of CMEs and the global density structure of the corona. The COSMO K-coronagraph science requirements were formulated by the COSMO Science Advisory Panel, the Mauna Loa User's Committee and HAO scientists. A listing of panel members is provided in the Acknowledgements. Science objectives have been translated into instrument requirements and goals in Table 1. Instrument requirements are summarized in Table 2. Science goals are discussed in more detail in Sections I and II.

Table 1: Science Requirements for the COSMO K-coronagraph

Science Requirements and Goals

Only the most strict requirement is listed

SCIENCE GOAL	QUANTITIES DETERMINED	INSTRUMENT REQUIREMENTS				
		FOV	PIXEL SIZE	CADENCE/ACCURACY	NOISE LEVELS	POINTING
Understand forces driving CMEs and related activity Distinguish CME models.	Time and location of CME onset. Evolution of CME basic properties (acceleration, mass, width …)	FOR ALL: Full FOV: 1.05 to 3.0 Solar Radii GOAL: 1.02	ALL: 6 arcsec	15 sec to capture dynamics of fast (v > 1000 k/s) CMEs GOAL: 8 sec. to minimize smearing of fastest CMEs CLOCK ACCURACY: 2 sec to minimize trajectory errors	FOR ALL SCIENCE GOALS: 2×10^{-09} B/Bsun in 15 sec with a S/N = 1 [= ~7.5×10^{-09} $pB_0 / \sqrt{Hz}$] GOAL: 3.4×10^{-10} B/Bsun in 8 sec, with a S/N=1	< 6 arcsec over 15 seconds
Solar cycle variation of coronal Temp. and B-field. Solar wind acceleration from coronal hole densities.	Change in density structure over low corona in open and closed field regions.					
Determine prominence role in CME formation	Early dynamics of CME and prominence activation and evolution.					
Detect Halo CMEs	Brightness, location and speed of halo CMEs			15 sec to capture dynamics of fast (v > 1000 k/s) CMEs		< 6 arcsec over 15 seconds
Particle Acceleration	Rate of change of CME acceleration, and density. Detection of associated waves.			15 sec to detect shock waves (v > 1000 k/s)		< 6 arcsec over 15 seconds

Quantity	Units	Requirement	Goal	Mk4
Field of view (FOV)	$D_\odot$	3	4	2.9
Lower Limit of FOV	Arcsec	50	25	120
Spatial Sampling	Arcsec	6	3	5 x 9 to 5 x 23
Noise Level	$pB_0 / \sqrt{Hz}$	7.5×10^{-9}	1.3×10^{-9}	5.4×10^{-8}
Map Time	sec	15	8	180
Pointing	Arcsec	<6 over 15 sec	<3 over 15 sec	

Table 2: Basic instrument requirements and goals are summarized for the COSMO K-coronagraph and compared to the existing Mauna Loa Mk4 K-coronameter.

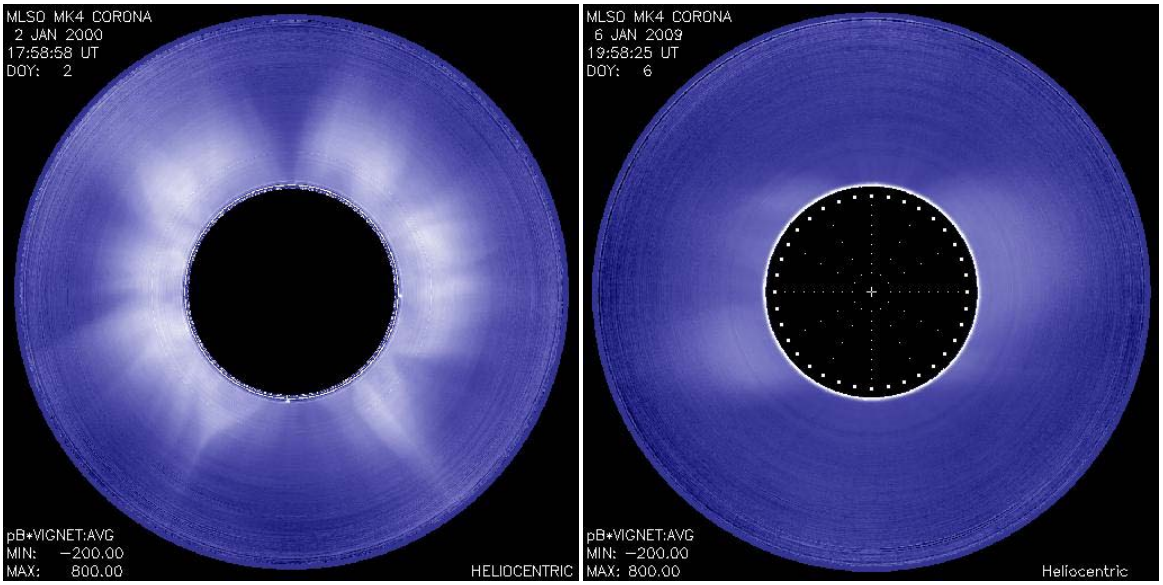

Figure 1. Comparison of coronal brightness between solar activity maximum (left) and activity minimum (right). Images were acquired with the MK4 Mauna Loa K-coronameter on Jan 2, 2000 during solar maximum and on Jan 6, 2009 during solar minimum. Brighter regions are locations where the Sun's magnetic field contains the plasma creating high density regions; dark regions are where the magnetic field is open, allowing the plasma and embedded magnetic field to escape to form the solar wind. Images have the same scaling and color table to illustrate solar cycle variations.

Section I. The White Light Corona

The density structure of the corona is arranged by the Sun's magnetic field into two regimes: closed-field high density and open-field low density regions. Knowledge of the density distribution provides important information on the morphology of the field and the location of solar wind outflows. Changes in the brightness of the corona over the solar cycle provides essential clues to the evolution of the global magnetic field and to the changes in the temperature and energy input to the corona over the activity cycle. Mechanical energy and momentum are deposited into the low corona-transition region which heats the corona to million degree temperatures and drives the solar wind. Observations of the density structure in the low corona are a crucial constraint on determining the location and amount of energy exchanged between the chromosphere and the corona. Radial density profiles, derived from white light brightness measurements,

are needed to determine; 1) magnetic field expansion factors; 2) the location where energy and momentum are deposited into the open field regions; 3) the location where the solar wind speed transitions to supersonic flow. White light brightness observations are also used to determine scale heights and estimate coronal temperatures. Images of the polarized brightness (pB) of the low corona have been observed at Mauna Loa since 1980

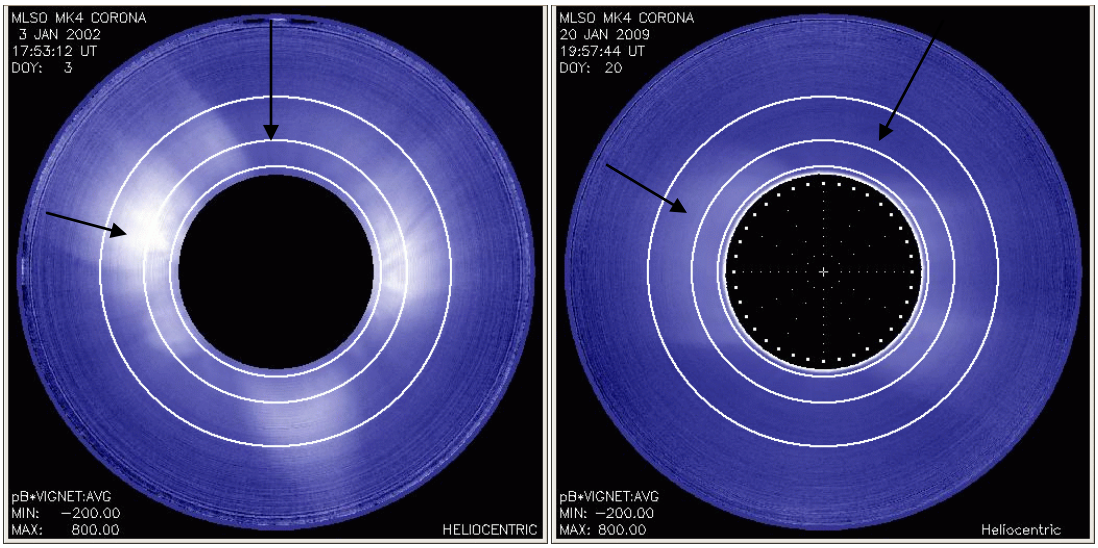

Figure 2. Polarization brightness images from Mauna Loa Mk4. At left: typical solar maximum image from Jan 3, 2002 and at right: solar minimum activity on Jan 20, 2009. White circles are at heights: 1.2, 1.5, and 2.0 R_o. The brightness at these heights is plotted in Figure 3. Arrows indicate examples of open and closed field structures. Radial brightness at these positions are plotted in Figure 4.

providing the community with important and unique observations (e.g. Cranmer et al. 1999, Guhathakurta et al. 1999, Bromage et al. 2000, Guhathakurta et al. 1993).

Polarization brightness images from Mauna Loa are shown in Figure 2 for solar maximum and solar minimum activity conditions. The variation in brightness between the two epochs is quantified in Figures 3 and 4. The brightness changes are due to a decrease in energy into the corona during solar minimum which lowers the average coronal temperature resulting in a smaller scale height and lower base density. Figure 3 displays the polarization brightness in units of brightness of the solar disk (B_o) as a function of position angle around the corona for 3 fixed heights: 1.2, 1.5 and 2.0 R_o, which are indicated by the white circles in the images in Figure 2. The peaks in brightness in Figure 3 are the locations of the closed field regions and the troughs are regions of open magnetic field. The figure shows that the brighter closed regions of the corona, at a given height, are between 3 and 5 times dimmer at solar minimum than at maximum, consistent with findings from previous datasets (e.g. Altrock et al.1999, MacQueen et al. 2001). The open field regions are between 5 and 10 times dimmer at minimum and drop below the noise level of the K-coronameter (~3.10^{-09}) at heights above 1.5 R_o at solar minimum and 2.0 R_o at solar maximum. 3-D models for the geometry and electron density, based on white light observations, indicate that the solar wind becomes supersonic between 2 and 3 R_o and energy and/or momentum are likely being deposited into the low corona from about 2 to beyond 5 R_o (Munro and Jackson 1977). Routine observations of open regions between 1.5 and 3.0 R_o are needed to better

understand the processes responsible for solar wind acceleration. ***The new coronagraph must observe over a sufficient dynamic range to record the brightest (~10^{-6} B_o) and the dimmest (< 10^{-9} B_o) coronal structures over the solar cycle with a polarization brightness accurate to 10%.***

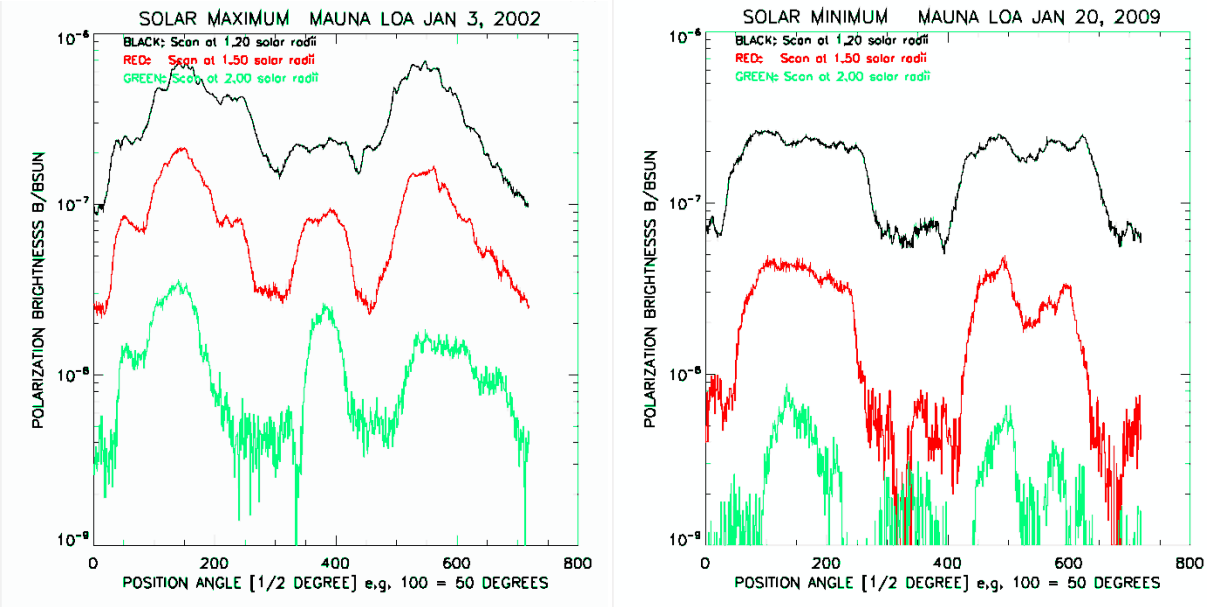

Figure 3. Log of brightness in units of the brightness of the solar disk (B_o)at 3 coronal heights: 1.2, 1.5 and 2.0 R_o at solar maxiumum (plot at left) on Jan 3 2002 and solar minimum (plot at right) on Jan 20, 2009.

The falloff in brightness with radius is examined in Figure 4. The position angle of the radial scans is indicated by the arrows in Figure 2. Figure 4 highlights the magnitude of the changes in radial brightness (and hence density) over the solar cycle between closed and open field regions. The log of polarization brightness in units solar disk brightess (B_o) is plotted vs. the log of the radial distance from sun center. Only data above the instrumental noise threshold of $3x10^{-9}$ B_o are plotted. Brightness falls rapidly with distance in this region of the corona, reflecting the rapid drop in density. Radial gradients vary between maximum and minimum and from open to closed field regions. The greatest variation in the radial gradient is in open regions between solar maximum and minimum, changing from $r^{-6.3}$ dependence at maximum to r^{-14} at minimum. The actual change is not as dramatic since the line-of-sight brightness integration at maximum very likely includes some closed field structures which exist at nearly all position angles at this phase of the cycle. The actual brightness decrease with radius in open regions at solar maximum is steeper than $r^{6.3}$. The current noise level limits brightness measurements in open field regions to ~1.45 R_o at solar minimum and ~2 R_o at maximum, well below the edge of the instrument field-of-view (FOV). The power law fits are extrapolated to lower brightness levels and show that a noise level of $1x10^{-09}$ B_o allows open field regions to be detected up to 2.5 R_o at maximum and 1.7 R_o at minimum. ***A noise level of $3x10^{-10}$ B_o permits the detection of the faintest coronal structures out to 2 R_o at solar minimum and up to 3 R_o at maximum utilizing the entire FOV. These images can be averaged over many minutes to achieve this goal.***

Images from the current Mk4 detector are averaged over 45 minutes to achieve a $3x10^{-9}$ B_o noise level in the far FOV.

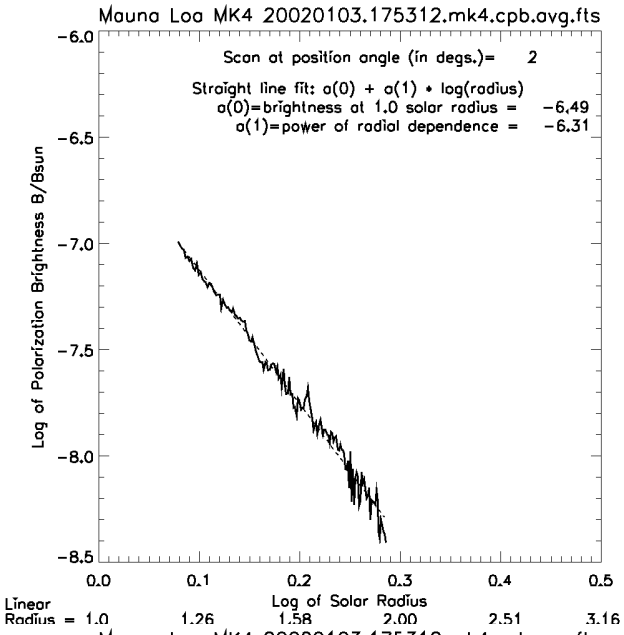

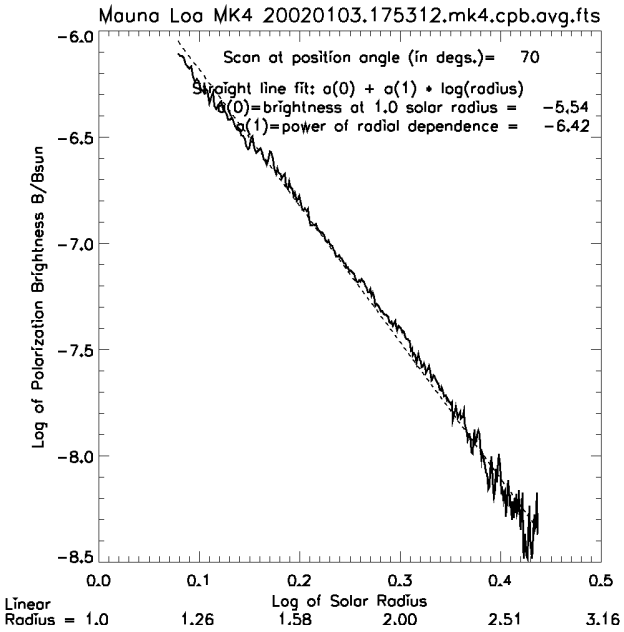

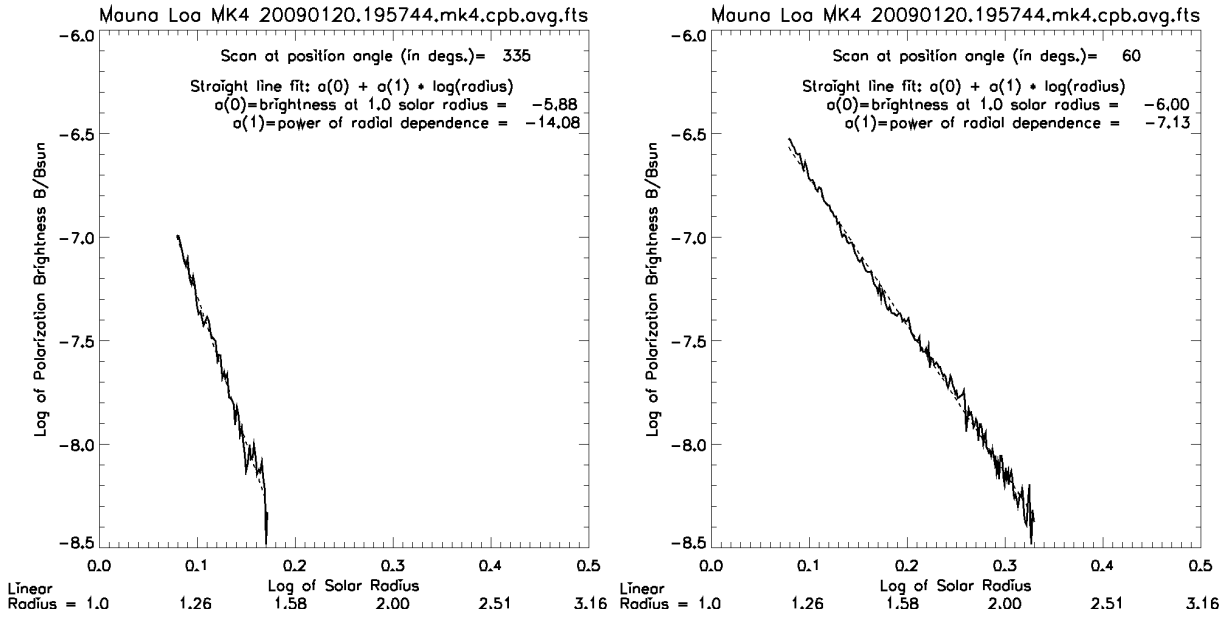

Figure 4. UPPER PANELS: Solar **Maximum** Corona on Jan 3, 2002. Upper left: open region (north pole), Upper right: closed region in northeast (60°). **LOWER PANELS**: Solar **Minimum** Corona on Jan 20, 2009. Lower left: open region (north pole); Lower right: closed region in northeast (60°). All plots are the log of polarization brightness in units of B_o vs log of radius. The dotted line in each plot is a power law fit to the data. The solar radius is given in both log and more familiar linear values.

Section II. CME requirements

CMEs are explosive events driven by magnetic stresses in the solar atmosphere and are the primary driver of space weather at earth. CMEs form and accelerate low in the corona with speeds and accelerations that can vary over 3 orders of magnitude. The greatest acceleration occurs below 3 R_o for most events. Observations of their onset and measurements of the rate-of-change of CME acceleration are needed to discriminate between the many models posited to explain their formation. ***This requires rapid image sequences of the very low corona with a field-of-view from 1.05 to 3.00 R_o to track CMEs from their formation in the first coronal scale height (1.01 to 1.09 R_o) to the height where they have acquired most of their acceleration (3 R_o).***

Accurate determinations of CME acceleration profiles require tens of measurements of the CME position over the FOV, and accurate clock information. Accurate timing is essential for determining the onset and accelerations of the fastest CMEs. ***The image time stamp with an accuracy of 2 seconds ensures that the uncertainty in the acceleration due to uncertainties in time is less than 5%.***

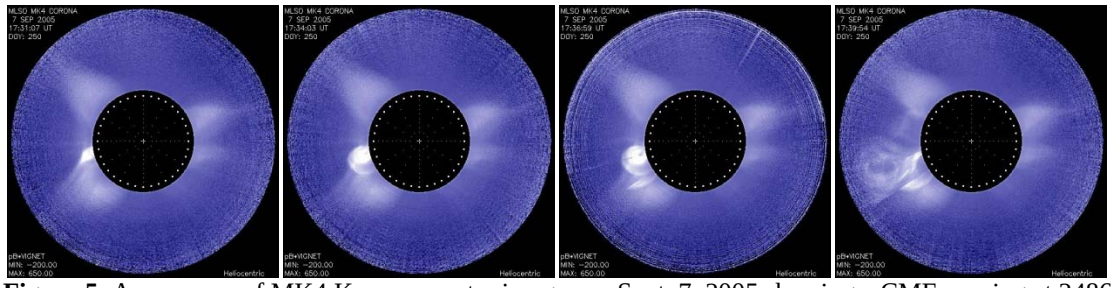

Figure 5. A sequence of MK4 K-coronameter images on Sept. 7, 2005 showing a CME moving at 2486 km/sec in the low corona. The CME is moving so rapidly that the front was detected in only 2 images (images 2 and 3 in this sequence). No acceleration could be measured.

The fastest CME recorded at Mauna Loa was traveling at 2486 km/sec or about 3.6 arcsec per sec and is shown in Figure 5. Mk4 images are acquired every 3 minutes which can be sufficient to determine constant accelerations of some CMEs but has proven to be insufficient to detect the rate-of-change of CME acceleration. Very high time cadence (13 to 40 sec) images recorded by TRACE and YOHKOH SXT have allowed measurements of acceleration changes over very limited heights (e.g. Alexander et al. 2002) for a very small number of events due to their limited FOV**. *15 second time cadence will provide tens of images per event that are needed to record accurate trajectories of the fastest CMEs.*** However, a 15 second integration would result in fast CMEs smearing across the coronagraph pixels (5.63 arcsec pixels) after a few seconds. A CME moving at 272 km/sec would take 15 seconds to traverse one pixel and would not smear. Table 3 shows the amount of pixel smearing vs. CME speed and the percentage of all observed LASCO CMEs with speeds below a given speed (derived from Mittal et al. 2009).The effect of smearing for the fastest Mauna Loa event is illustrated in Figure 6. Smearing effects on highly structured prominences are shown in Figure 7.

CME speed (k/s)	**CME speed (arcsec/s)**	**# of 5.63 arcsec pixels smeared in 15 seconds**	**% of all LASCO CMEs below the speed in column 1**
272	0.375	1	21 %
544	0.751	2	77%
1088	1.502	4	96%
1632	2.253	6	98%
2176	3.003	8	99.6%
2720	3.754	10	99.9%

Table 3 : A list of CME speeds and the amount of smearing (in pixels) that would occur over a 15 second integration time. The rightmost column displays the percentage of all LASCO CMEs that are moving at or below the speed listed in the lefthand column. Nearly all CMEs move at speeds below 1000 k/s. Clarity of CME features will be maintained for nearly all CMEs observerd.

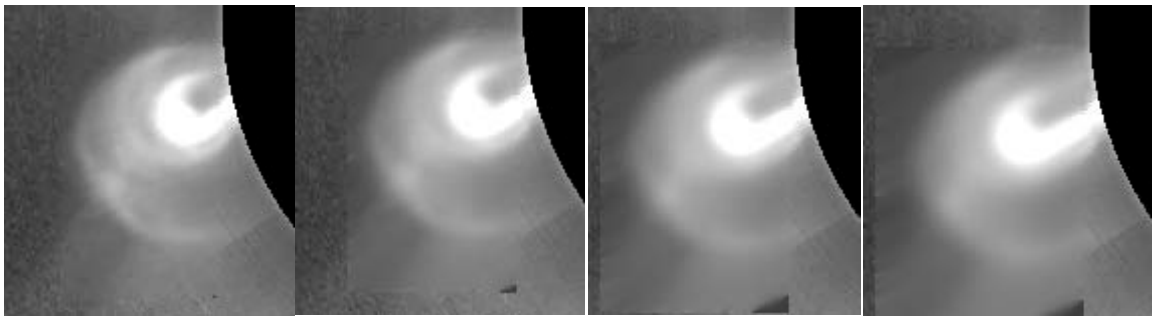

Figure 6. CME from Sep 7, 2005 but smeared across pixels to simulate longer integration times. This CME is moving at 2486 k/s or ~0.61 pix/sec. Leftmost image is smeared across **2 pixels** which is equivalent to an integration time of 3.3 seconds; next figure is smeared **5 pixels** (8.2 sec); second from right is smeared **10 pixels** (16.4 sec); and the rightmost is smeared **15 pixels** (24.6 sec).

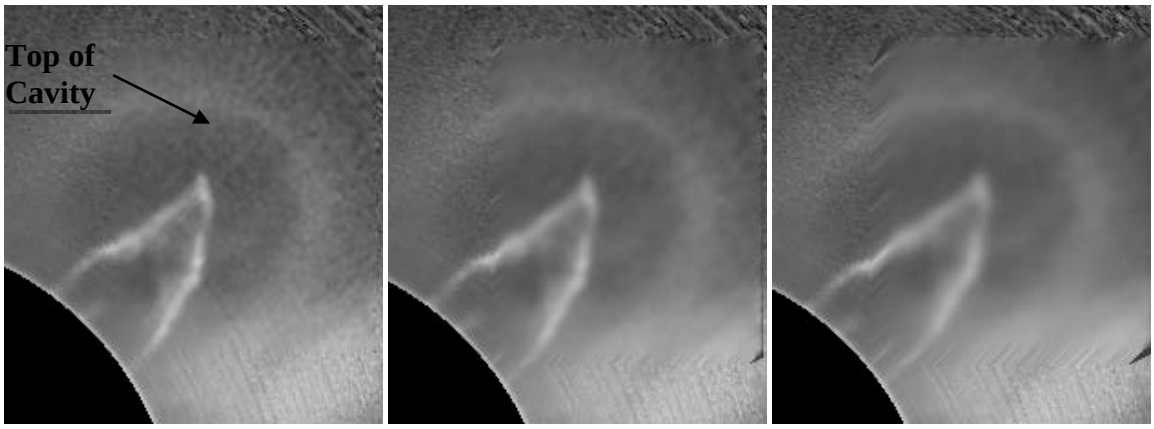

Figure 7. Smearing of CME from Feb 18, 2003 to illustrate the effect of smearing on highly structured prominences. The figure on the left has been smeared **2 pixels**; the image in the center has been smeared **5 pixels** and the image at far right has been smeared **10 pixels**. Some of the fine structure begins to be lost in the 10 pixel smear but the top of the dark cavity and the outer loop are still detectable.

CME structures such as the prominence, cavity and front are still detectable over 10 pixel smearing. ***A 15 second integration time will accommodate 99% of all CME speeds (see Table 2). A goal of 5 pixel smearing (8 second cadence) will reduce the level of blurriness in fast moving CMEs enabling the detection of fine structure visible in many erupting prominences. Stable pointing is essential in order to avoid additional smearing of images during integrations. Accurate pointing to within a pixel is needed leading to a pointing requirement of 5.6 arcsec RMS over 15 second integrations.***

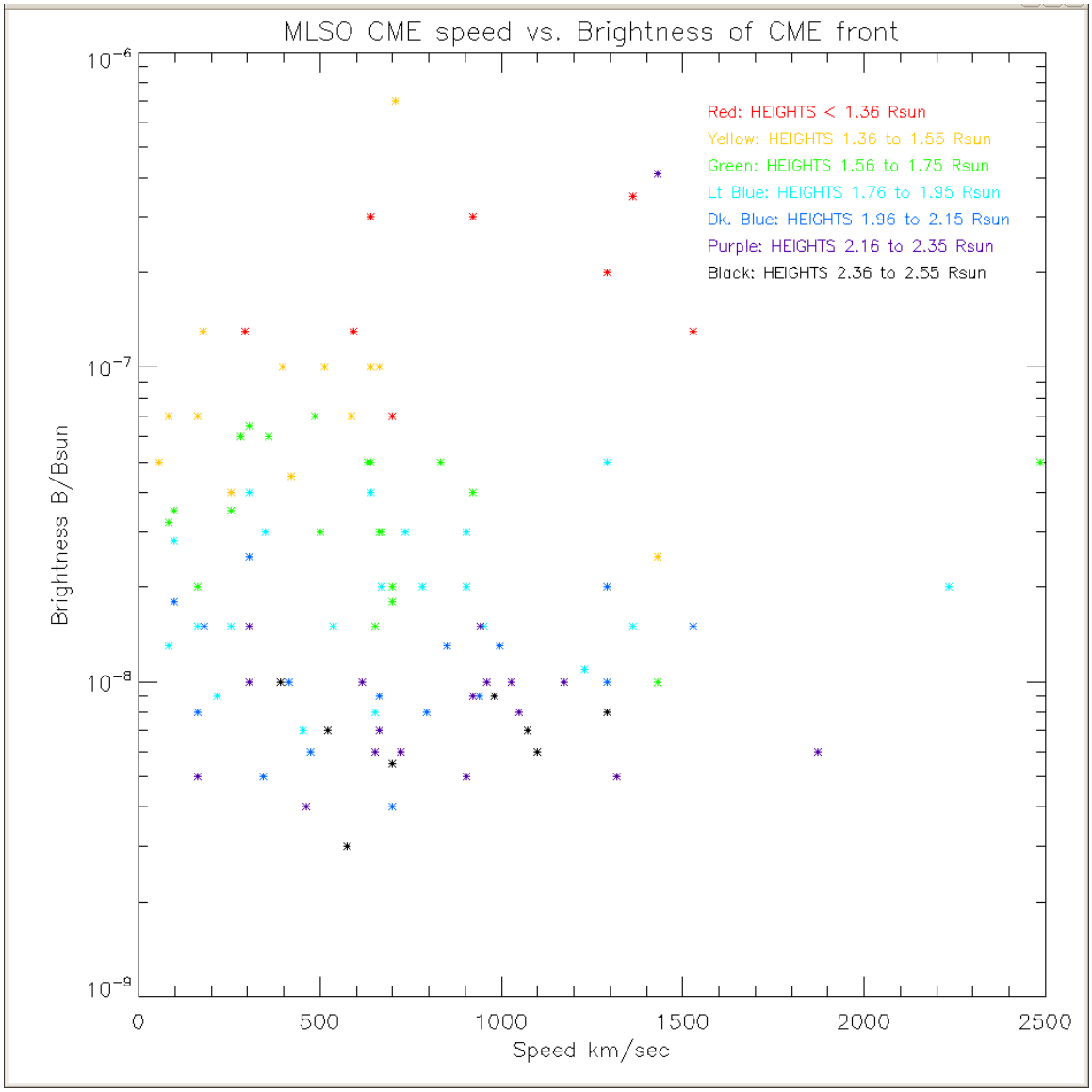

Figure 8. CME brightness and speed measurements for 31 MK4 CMEs. Data are color coded as a function of CME height to show the brightness requirements over the coronagraph FOV. The MK4 noise level is $3x10^{-09}$ B_o.

CME Brightness

An integration time of 15 seconds is sufficient to capture CME acceleration profiles for most events within the required FOV without adverse pixel smearing, but is this integration time sufficient to provide the brightness levels needed to detect CMEs? We examine the brightness levels of a selection of MK4 CMEs as a function of CME speed and height as shown in Figure 8. The large scatter in Figure 8 confirms there is no obvious correlation between CME speed and brightness. Brightness is a strong function of CME height as shown by the color coding. What is not shown, but is well known, is that brightness is also a strong function of CME distance from the solar limb. CMEs occurring far from the limb (e.g. halos) are significantly fainter due to projection effects. The faintest CMEs in Figure 8 have brightnesses of ~$3x10^{-9}$ B_o which is the noise limit of the MK4 camera and not a property of CMEs. This noise threshold is too high to detect

most halo events and other faint structures. MK4 has recorded fragments of brighter halos such as the Feb 17, 2000 halo event shown in Figure 9 in LASCO observations. The halo section over the south pole was recorded in MK4 with a brightness of $4x10^{-9}$ $B_\odot$ at 2.0 $R_\odot$. ***A noise level of $1x10^{-9}$ $B_\odot$ is needed to detect faint CMEs out 3 $R_\odot$. A noise level of $3x10^{-10}$ $B_\odot$ will permit the detection of a large fraction of halo events that are currently visible in the LASCO coronagraphs at these brightness levels but are undetectable by the MK4 K-coronameter. These brightness requirements are identical to those of the ambient coronal structures from which CMEs form. A spatial resolution of 6 arcsec permits the tracking of highly structured prominence features such as those depicted in Figure 7.***

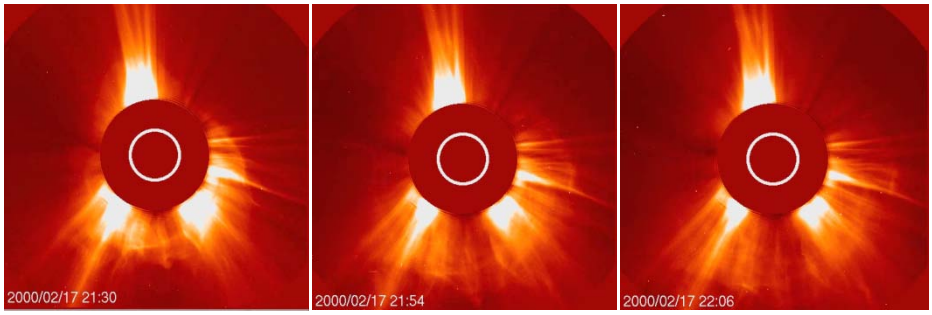

Figure 9. LASCO halo CME of February 17, 2000. The portion of the halo directly over the south pole was recorded by the MK4. The brightness of the halo at 2.0 $R_\odot$ was $4x10^{-9}$ $B_\odot$. This is one of the brighter halos recorded by LASCO.

Conclusion

The COSMO K-coronagraph instrument requirements listed in Table 1 will allow it to detect accleration profiles of CMEs, identify many halo CMEs, and observe open and closed coronal structures over the full field-of-view for most solar activity cycle conditions.

Acknowledgements

HAO scientists which to express their appreciation to the members of the COSMO science advisory panel and to the Mauna Loa User's committee for contributing their time and expertise to the COSMO project and to the Mauna Loa Solar Observatory. Their efforts were invaluable in producing clear and concise science goals for the COSMO K-coronagraph and informulating a strategic plan for the Mauna Loa Solar Observatory based on community needs.

COSMO Science Advisory Panel:
Thomas Zurbuchen, University of Michigan (Chair)
David Alexander, Rice University
Spiro Antiochos, NASA Goddard Space Flight Center
Jean Arnaud, Université de Nice, France
Phil Judge, High Altitude Observatory, NCAR
Matt Penn, National Solar Observatory
John Raymond, Harvard Smithsonian Center for Astrophysics

Aad VanBallegooijen, Harvard Smithsonian Center for Astrophysics

Mauna Loa User's Committee:
David Alexander, Rice University (Chair)
Nick Arge, Air Force Research Laboratory
Tim Bastian, National Radio Astronomy Observatory
Terry Forbes, University of New Hampshire
Holly Gilbert, NASA Goddard Space Flight Center
Shadia Habbal, University of Hawaii IfA
Jerry Harder, University of Colorado, LASP
Alex Pevtsov, National Solar Observatory
Chris St.Cyr, NASA Goddard Space Flight Center

References

Alexander, David, Thomas R. Metcalf, Nariaki V. Nitta, 2002, Fast acceleration of a CME-related X-ray structure in the low solar corona, Geophys. Res. L., 29, 10, pp 41-1

Altrock, R.C., M. Rybansky, V. Rusin, M. Minarovjech, 1999, Determination of the solar minimum period between cycles 22 and 23 from coronal index of solar activity, Solar Phys., 184, 317-322

Bromage, B. J. J., D. Alexander, A. Breen, J.R. Clegg, G. Del Zanna, C. DeForest, D. Dobrzycka, N. Gopalswamy, B. Thompson, and P.K. Browning. (2000), "Structure of a large low-latitude coronal hole", *Solar Phys.***, 193**, 181-193.

Cranmer, S. R., J. L. Kohl, G. Noci, E. Antonucci, G. Tondello, M. C. E. Huber, L. Strachan, A. V. Panasyuk, L. D. Gardner, M. Romoli, S. Fineschi, D. Dobrzycka, J. C. Raymond, P. Nicolosi, O. H. W. Siegmund, D. Spadaro, C. Benna, A. Ciaravella, S. Giordano, S. R. Habbal, M. Karovska, X. Li, R. Martin, J. G. Michels, A. Modigliani, G. Naletto, R. H. O'Neal, C. Pernechele, G. Poletto, P. L. Smith, and R. M. Suleiman. (1999), "An Empirical Model of a Polar Coronal Hole at Solar Minimum", *Astrophys.J.***, 511**, 481-501

Gosling, J.T., E. Hildner, R.M. MacQueen, R.H. Munro, A.I. Poland and C.L. Ross, 1976, The speeds of coronal mass ejection events, Solar Phys., 48, 389-397

Guhathakurta, M., A. Fludra, S. E. Gibson, D. Biesecker, and R. Fisher. (1999), "Physical properties of a coronal hole from a coronal diagnostic spectrometer, Mauna Loa coronagraph, and LASCO observations during the Whole Sun Month", *Journal of Geophysical Research***, 104 A5**, 9801

Guhathakurta, M., R. R. Fisher, and R. C. Altrock. (1993), "Large-Scale Coronal Temperature and Density Distributions, 1984-1992", *Astrophysical Journal***, 414**, L145-L148

Howard, R.A., N.R. Sheeley, Jr., D.J. Michels, M.J. Koomen, 1985, Coronal mass ejections – 1979-1981, J. Geophys. Res., 90, 8173-8191

Hundhausen, A.J., J.T. Burkepile, O.C. St.Cyr, 1994, Speeds of coronal mass ejections : SMM observations from 1980 and 1984-1989, J. Geophys. Res., 99, 6543-6552

Hundhausen, A.J., 1993, Sizes and locations of coronal mass ejections – SMM observations from 1980 and 1984-1989, J. Geophys Res., 98, 13177-13200

MacQueen, R.M., J.T. Burkepile, T.E. Holzer, A.L. Stanger, K.E. Spence, 2001, Solar Coronal Brightness Changes and Mass Ejections during solar cycle 22, Astrophys. J., 549, 1175-1182

Mittal, Nishant, Joginder Sharma, Vivek Tomar, Udit Narain, 2009, On distribution of CMEs speed in solar cycle 23, Planetary and Space Science, Vol 57, pp 53-57

Munro, R. H., B.V. Jackson, 1977, physical properties of a polar coronal hole from 2 to 5 solar radii, Astrophys., J., 213, 874-886

Schmit, D.J., S. Gibson, G. deToma, M. Wiltberger, W.J. Hughes, H. Spence, P. Riley, J.A. Linker, Z. Mikic, 2009, A novel metric for coronal MHD models, J. Geophys. Res., 114, A6, A06101

St.Cyr, O.C., J.T. Burkepile, A.J. Hundhausen, A.R. Lecinski, 1999, A comparison of ground-based and spacecraft observations of coronal mass ejections from 1980-1989, J. Geophys. Res., 104, 12493-12506

Yashiro, S., N. Gopalswamy, G. Michalek, O.C. St.Cyr, S.P. Plunkett, N.B. Rich, R.A. Howard, 2004, A catalog of white light coronal mass ejections observed by the SOHO spacecraft, J. Geophys. Res., 109, A7, A07105